Enhancement of grain structure and mechanical properties of a high-Mn twinning-induced plasticity steel bearing Al-Si by Fast-Heating Annealing

Ali Khosravifard [a], Atef Hamada [b,*], Antti Järvenpää [b], Pentti Karjalainen [c]

[a] Metallurgical and Materials Engineering Department, School of Engineering, Shiraz Branch, Islamic Azad University, Box 71993-1, Shiraz, Iran

[b] Kerttu Saalasti Institute, University of Oulu, Pajatie 5, 85500 Nivala, Finland

[c] Centre for Advanced Steels Research, University of Oulu, Box 4200, 90014 Oulu, Finland

Abstract

In this study, a cold-rolled Fe-0.01C-21.3Mn-3Al-3Si (wt.%) TWIP steel was undergone a fast-heating (FH) annealing at high temperatures of 1000–1200 °C and 2 s soaking time for grain refinement and controlling the phase structure and thereby to enhance the mechanical properties. For comparison, recrystallization annealing was conducted at lower temperatures of 650 and 700 °C for 180 s. The microstructural evolution of the FH annealed steel was surveyed using electron backscatter diffraction. The strain hardening behavior of the FH structures was studied by tensile tests. The tensile flow curves were also predicted by a phenomenological model based on the evolution of dislocation density during deformation. Fine mainly austenitic structure was promoted by FH annealing at 1000 and 1100 °C. At the lower temperatures of 650 and 700 °C, bands of finer grains, indicative of some inhomogeneity, were evident in the mostly austenitic recrystallized microstructure. However, at 1200 °C, the structure consisted of coarse austenite and ferrite with almost equal fractions. The FH annealed structures exhibited a remarkable improvement in the mechanical properties (a better combination of yield and tensile strength and ductility) compared to conventional long annealing cycles.

Keywords:

High-Mn TWIP steel; fast-heating annealing; grain structure; tensile strength; phase transformation; phenomenological model.

* Corresponding author: Atef Hamada

E-mail: atef.hamadasaleh@oulu.fi (A.S. Hamada).

Introduction

Fast-heating (FH) annealing is a new technology for heating a steel with a heating rate higher than 100 °C/s. This technology is developed to establish a new processing route in the steel industry to control the recrystallization kinetics of the cold-rolled material and consequently its grain structure [1, 2, 3]. Moreover, FH annealing is a promising technique also in reducing energy consumption and improving the mechanical properties of the products. In this context, Meng et al. [4] applied the FH annealing, *i.e.* a heating rate of 500 °C/s and a soaking time of 2 s, on a cold-rolled dual-phase steel DP590 and found an improvement in both the strength and ductility. Also, the influence of ultrafast annealing on DP780 steel is recently studied by Vercruysse et al. [5] who found that heating rates of up to 1000 °C/s considerably increased the energy absorption potential of the material. Xu et al. [6] studied the influence of heating rate on the microstructure and mechanical properties of an Fe-0.2C-1.8Mn-1.5Si (in wt.% hereafter) TRIP steel. They reported an increased austenite content in the TRIP steel when applying higher heating rates of up to 500 °C/s. In a following work, the same research group [7] employed FH annealing (300 °C/s) to achieve the intercritical annealing of a cold-rolled quenching and partitioning (Q&P) steel with the chemical composition Fe-0.21C-1.40Si-1.30Mn. It was found that when the heating rate is increased, grain refinement is promoted and bainite transformation suppressed. De Knijf et al. [8] studied the effect of ultra-fast annealing with high heating rates of 500 and 1000 °C/s on the microstructural evolution and the correlated mechanical properties of a Q&P steel. The mechanical properties were significantly improved and the fracture appearance was changed from brittle cleavage to ductile dimples when the heat treatment was performed at high heating rates. In a recent work, applying ultrafast heating with various rates on an Fe-0.19C-1.61Mn-1.06Al-0.5Si steel showed that nanohardness of the martensitic constituent considerably depended on the heating rate while ferrite showed an ignorable sensitivity [9]. Also, in an ongoing research project, the University of Oulu is involved with a steel manufacturer to adopt FH annealing in an industrial line by applying High-Frequency Induction Technology. The effect of supreme heating rates (1000–10,000 °C/s) and a short annealing cycle on the mechanical properties of carbon steels, along with the influence on phase constituents, chemical uniformity and residual stresses are under investigation.

Ueji et al. [10] studied the twinning behavior of an Fe-31Mn-3Al-3Si TWIP steel with various grain sizes in the range 1.8–50 μm and observed a significant suppression of deformation twinning with

grain refinement. In a similar work, Rahman et al. [11] investigated five different grain sizes in an Fe–0.17C-15Mn–2Al–2Si TWIP steel and found that the yield stress was increased with decreasing the grain size, while ductility was not considerably altered. Furthermore, the stress required for the initiation of twinning showed a reverse relationship with grain size. A combination of high yield strength (785 MPa) and excellent elongation (48%) has been obtained in a fully recrystallized ultrafine-grained Fe-0.6C-22Mn TWIP steel [12]. The steel was shown to obey the Hall-Petch relationship in a wide range of grain size from coarse to ultrafine. Yuan et al. [13] investigated the influence of annealing on an Fe-25Mn-3Cr-3Al-0.3C-0.01N TWIP steel and found that increased annealing temperature resulted in a higher density of $\Sigma 3$ grain boundaries and mechanical twins. Lan and Zhang [14] studied the effect of annealing time and temperature on the mechanical properties of an Fe-22Mn-0.5C TWIP steel. They showed that in order to attain a high combination of strength and ductility, a certain range of grain size should be achieved during the annealing process. Also, very high strength and ductility are recently reported due to formation of nano-twins in a TWIP steel undergone ultra-rapid heat treatment [15]. Wang et al. [16] applied a laser heat treatment on a cold-rolled (Fe-30Mn-3Al-3Si) TWIP steel to fabricate a grain size gradient structure throughout the cross section, depending on the fast heating and cooling of the laser beam. On the other hand, similar studies have been conducted on the steels with a mixed TRIP/TWIP behavior. In this regard, Dastur et al. [17] annealed a cold rolled Fe-0.07C-18Mn-2Al-2Si steel in a range of temperature (500–920 °C) and duration (10–3600 s). It was seen that higher annealing temperatures with shorter durations resulted in finer grain sizes (down to 800 nm) where the austenite to martensite transformation in tensile tests at ambient temperatures was delayed to higher strains leading to improved ductility. Also, Lee et al. [18] showed that the critical resolved shear stress for martensitic transformation is more sensitive to grain size than that for twinning. Thus, it was suggested that a transition from TWIP to TRIP may occur with grain coarsening.

Modeling the mechanical behavior of TWIP steels has also been the subject of some recent research work. In this regard, various models including empirical and physically based equations have been developed. Physical models usually contain several parameters to be identified. It has been shown that identification of the model parameters from the material's macroscopic behavior requires especial considerations [19]. However, these models give a better understanding of the correlation between the mechanical behavior of the material and its microstructural features [20]. In this regard, some physically based models have been utilized in recent researches related to austenitic TWIP

type steels. Kang et al. [21] employed the Kocks and Mecking model to predict the dislocation density during tensile deformation of TWIP steels in the temperature range 23–110 °C. Also, Liu et al. [22] studied the influence of temperature on strain hardening capability of TWIP steel based on a physical model considering dislocations and mechanical twins. Furthermore, in order to cover high rate deformations of TRIP and TWIP steels, Joo and Huh [23] developed an isotropic-kinematic hardening model which included the effect of strain rate. The model for instance was able to predict the springback of sheet metal in high strain rate forming processes.

Critical review of the open literature as mentioned above shows that the influence of FH processing on the grain structure and the resultant mechanical behavior has been studied for some carbon steels, dual phase steels and quenching & partitioning steels. However, the FH annealing has not yet been reported in the open literature for any composition of high-Mn TWIP steels.

The present work investigates the effect of FH annealing on a cold-rolled high-Mn TWIP steel bearing 3%Al and 3%Si (wt.%) in a range of temperatures 1000–1200 °C by applying a high heating rate (~200 °C/s) and short soaking times of 2 s. Lower annealing temperatures (650700 C) with longer duration of 180 s are also examined and compared. The influence of the FH treatment on the microstructural evolution and its concurrent effect on the mechanical strengths is studied. Furthermore, the applicability of the well-known dislocation density-based Bergstrom's equations to predict the flow curves of annealed samples is evaluated.

2. Material and Methods

2.1. Material

The studied TWIP steel was received in the form of 20 mm thick cast ingots with a chemical composition of Fe-0.01C-21.3Mn-3Al-3Si. The steel was laboratory cast using vacuum induction melting at Centro Sviluppo Materiali (CSM), Rome, Italy. Based on the thermo-dynamical model originally introduced by Olson and Cohen [24], the stacking fault energy (SFE) of this steel is calculated to be 19.4 mJ/ m^2 at room temperature and thus is situated in the range of dominance of the TWIP mechanism. The detailed procedure of SFE calculation is explained in a previous work [25].

The cast ingots were homogenized at 1100 ℃ for 2 hours to remove the segregation of alloying elements, especially Mn. Subsequently, they were hot rolled to 5 mm thick bands and then cold rolled to a final thickness of 2 mm in a laboratory rolling mill, so that a 60 % reduction in thickness equivalent to a true strain ≈ 1 was applied.

2.2 Fast-heating annealing process

The cold-rolled sheets were FH annealed using a Gleeble thermo-mechanical simulator which would apply a high heating rate (~ 200 °C/s) by resistance heating and almost the same cooling rate by accelerated air blowing. The FH annealing was carried out at different temperatures of 1000 to 1200 °C and a soaking duration of 2 s. The thermo-mechanical schedule and FH annealing cycle are schematically shown in Fig. 1. For comparison, low temperature annealing treatments at 650 and 700 °C for longer time of 180 s were conducted using the same heating and cooling rates.
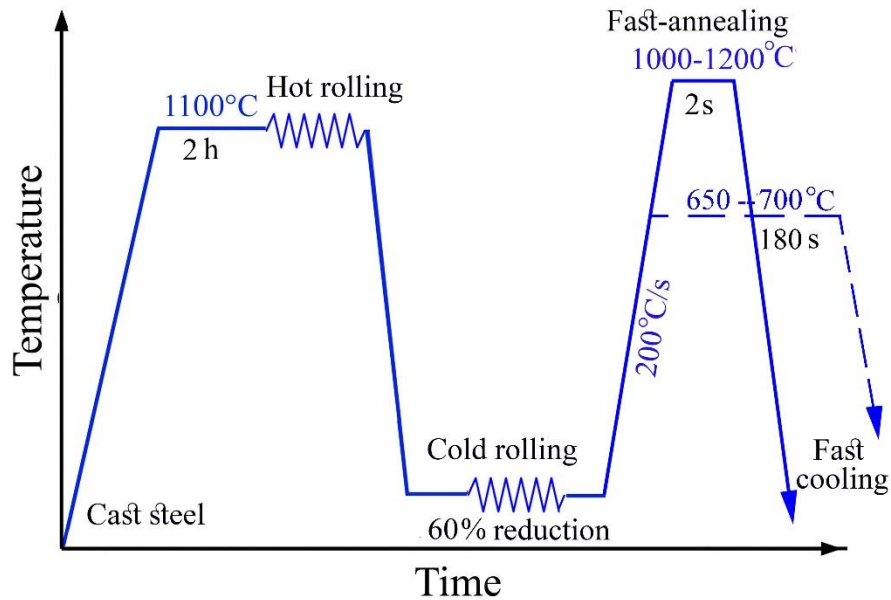
Fig. 1. Schematic of the thermo-mechanical schedule used for fast-heating annealing of the cold-rolled TWIP steel.

2.3. Tensile and hardness tests

The quasi-static mechanical properties at room temperature of the obtained microstructures were measured using uniaxial tensile tests at a strain rate of 10^{-3} s^{-1} on a Zwick Z 100 tensile machine (Zwick Roell, GmbH). Sub-sized tensile testing specimens were machined according to ASTM E-8 with a gage length of 32 mm, a width of 6 mm and a total length of 130 mm.

Microhardness of the austenite and ferrite phases was determined using a Vickers hardness tester under the load of 500 g.

2.4. Microstructural studies

The initial cast microstructures of the steel were studied using a light optical microscope. In addition, a field-emission gun scanning electron microscope (FEG-SEM) was utilized to obtain further details of the cast and recrystallized microstructures. In order to survey the distribution of alloying elements in the cast specimens, they were analyzed by an energy dispersive spectroscope (EDS) unit. On the other hand, the microstructures achieved after applying the annealing cycles to the cold-rolled steel were examined by an electron backscatter diffraction (EBSD) detector in a FEG-SEM. An acceleration voltage of 15 kV was used during the EBSD scans. Furthermore, a Ferritscope (Helmut Fisher MP30) instrument was used to quantify the fraction of the ferromagnetic α-ferrite phase among the non-ferromagnetic γ-austenite. The phase constituents of the cast material and the FH annealed structures were also examined by X-ray diffraction (XRD).

2.5. Modeling the mechanical behavior

The room temperature flow stress of the steel after different recrystallization time/temperature conditions was predicted by a phenomenological model which correlates the flow stress with the evolution of dislocation density. The flow stress at the onset of deformation only depends on the lattice friction stress. But, during straining, it is also affected by both isotropic and kinematic strain hardening. Thus, the flow stress can be simply considered as $\sigma = \sigma_0 + \sigma_1 + \sigma_2$, where σ_0 is the lattice friction stress which (at constant temperature and strain rate) depends only on the chemical composition; σ_1 represents the increase in flow stress due to isotropic hardening which is caused by

the non-directional influence of dislocations accumulation; and σ_2 is the contribution of the internal stresses of the material which is also known as the Bauschinger effect. It has been shown that this effect has considerable influence on the flow stress of TWIP steels especially at low strain rates [26].

Isotropic hardening (σ_1) is a function of the square root of dislocation density (ρ) as represented by Eq. (1).

$$\sigma_1 = \alpha GbM \sqrt{\rho} \tag{1}$$

where α is a constant related to the efficiency of dislocation strengthening, G is the shear modulus of elasticity, b is the magnitude of burgers' vector, and M is the average Taylor factor. The variations of dislocation density during deformation is the result of a competition between dislocations accumulation and annihilation.

For FCC regions, the accumulation of dislocations is modeled based on the statistical method of Kocks and Mecking [27], while the dislocation annihilation is considered according to the equation suggested by Estrin and Mecking [28]. As the consequence, the variation of dislocation density with strain (ε) can be written as follows:

$$\frac{d\rho}{d\varepsilon} = M.(\frac{1}{bL} + H\sqrt{\rho} - R.\rho) \tag{2}$$

In the above equation, H and R are the hardening and recovery parameters, respectively and L is a length scale parameter depending on the microstructure. In austenitic regions where mechanical twinning occurs during deformation, L depends on both the average grain size (d) and average twin spacing (λ) [22]:

$$\frac{1}{L} = \frac{1}{d} + \frac{1}{\lambda} \tag{3}$$

As the deformation progresses, the volume fraction of mechanical twins (F) increases and hence the parameter λ decreases. The relation between these two has been obtained by an stereological analysis [29] and can be written as Eq. (4).

$$\frac{1}{\lambda} = \frac{1}{2t} \frac{F}{1-F}$$ (4)

where t is the average thickness of mechanical twins. On the other hand, the relationship between the twin volume fraction (F) and the applied true strain (ε) was considered in the form an empirical equation as follows:

$$F = F_0(1-\exp(-\beta(\varepsilon - \varepsilon_i)))^m$$ (5)

where β and m are constants, F_0 is the maximum volume fraction of the twins, and ε_i is the true strain for initiation of mechanical twinning in the microstructure. Finally, the contribution of kinematic hardening (σ_2) in the flow stress of the material was considered according to Eq. (6) [28].

$$\sigma_2 = M \frac{Gbn}{L}$$ (6)

The parameter n in Eq. (6) represents the number of dislocations piled-up at obstacles (grain boundaries and twins). The variation of n with ε was extracted from [29] as follows:

$$\frac{dn}{d\varepsilon} = \frac{w}{b}(1-n/n_0)$$ (7)

where w/b is the number of geometrically necessary dislocations for each slip band, and n_0 is the maximum number of dislocation loops at each obstacle.

The microstructure of the studied steel after annealing recrystallization consisted of a fraction of ferrite in addition to austenite. For the calculation of kinematic hardening (σ_2), the same equation as that used for austenite, i.e. Eq. (6), was used for ferrite, too. But, considering the fact that mechanical twinning is not expected in ferritic regions, the length scale parameter (L) was set equal to the grain size (d) for ferrite.

On the other hand, another approach was used for the isotropic hardening (σ_1) of ferrite. In this method which is based on the well-known Bergstrom's equation, the variation of dislocation density with the applied strain is given as follows:

$$\frac{d\rho}{d\varepsilon} = U - \Omega\rho$$ (8)

where U and Ω are the hardening and softening parameters, respectively. Both parameters are assumed to be independent of the applied strain [30]. Thus, the dislocation density can be obtained by integration of Eq. (8) with the initial condition of $\rho = \rho_0$ for $\varepsilon = \varepsilon_0$:

$$\rho = \rho_0 \exp(-\Omega\varepsilon) + \frac{U}{\Omega}(1 - \exp(-\Omega\varepsilon)) \tag{9}$$

The detailed procedure of calculating the dislocation density from Eq. (9) is described in a previous work [31]. By inserting ρ from Eq. (9) into Eq. (10), the contribution of isotropic hardening for ferrite is determined.

$$\sigma_1 = \alpha' Gb\sqrt{\rho} \tag{10}$$

where α' is the dislocation strengthening constant. Therefore, in case of dual phase specimens, σ_1 and σ_2 were determined separately for austenite and ferrite phases. Consequently, the flow stress for these specimens was calculated through Eq. (11).

$$\sigma = \sigma_0 + f_{fer}.(\sigma_{1,fer} + \sigma_{2,fer}) + f_{aus}.(\sigma_{1,aus} + \sigma_{2,aus}) \tag{11}$$

where f_{fer} and f_{aus} are the fractions of ferrite and austenite. Finally, a MATLAB code was developed to solve the differential equations and fit the model on the experimental data of the tested specimens.

3. Results

3.1. Microstructures of the cast material

The cast microstructure of the steel Fe-0.01C-21Mn-3Al-3Si is shown in Fig. 2. Columnar dendritic morphology, typical of cast materials is obvious in Fig. 2(a). However, irregularity is also a conspicuous feature of the cast microstructure. The structure consists of austenite γ-*fcc* + ferrite α-*bcc* phases, as seen at a higher magnification in Fig. 2(b). Ferrite is present with two morphologies, ferrite laths at austenite grain boundaries and vermicular ferrite within the austenitic grains. It can be observed that the columnar dendritic pattern consists of austenite in the dendritic cores and arms

and ferrite located in interdendritic regions. The presence of the above-mentioned phases was also confirmed by XRD, as shown in Fig. 3.
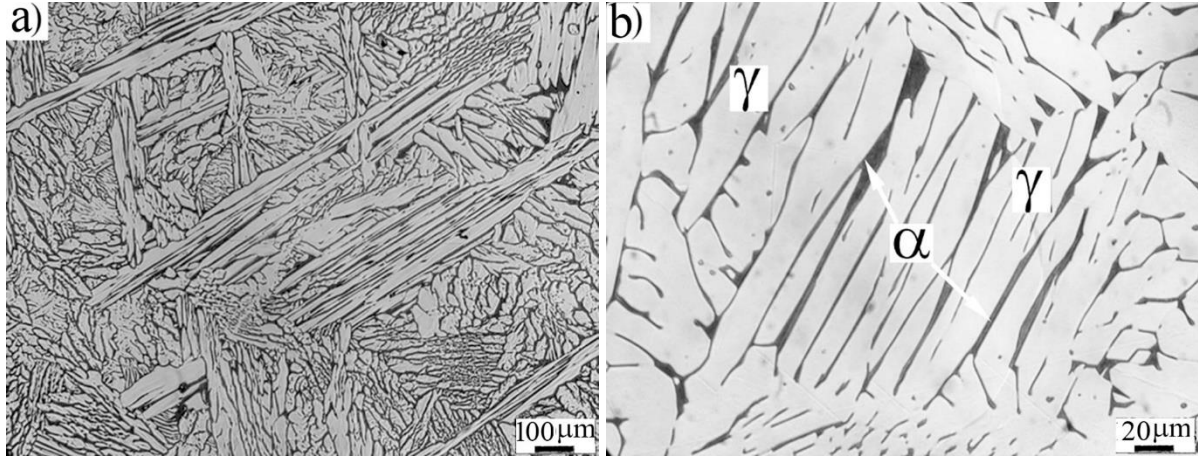

Fig. 2. Optical microstructures of the as-cast steel: (a) typical dendritic morphology, (b) lathy ferrite (black) located between the austenite columns and vermicular ferrite inside the austenite phase.
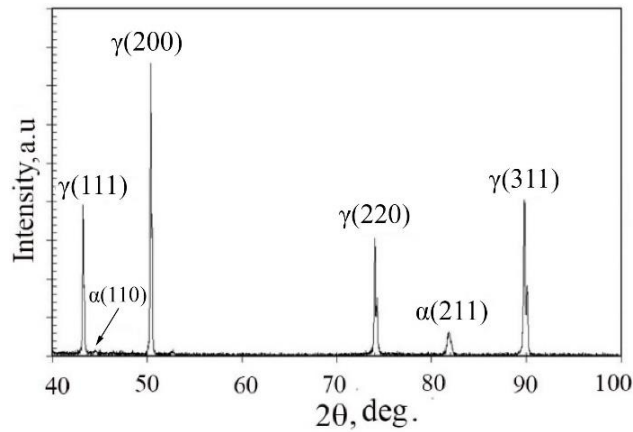

Fig. 3. XRD pattern of the cast steel confirming the presence of duplex structure.

3.2. Microstructural evolution during FH annealing

The microstructures examined by EBSD after cold rolling and subsequent annealing at 650 and 700 °C for 180 s are depicted in Fig. 4. According to Fig. 4a, the microstructure after annealing at 650 °C reveals an ultrafine-grained austenite structure (in grey color) with a small fraction of ferrite

(blue areas) formed on austenite grain boundaries. The grain size distribution obtained from EBSD analysis (Fig. 4(b)) shows that about 85% of the grains are smaller than 1 µm with the average grain size of 0.8 µm. A very similar structure with almost the same amount of ferrite was seen after annealing at 700 °C (Figs. 4(c) and (d)). This is in agreement with the measurements of ferrite content by the Ferritscope instrument, as presented in Table 1. The grain size values in this table are the average obtained from the EBSD analysis.
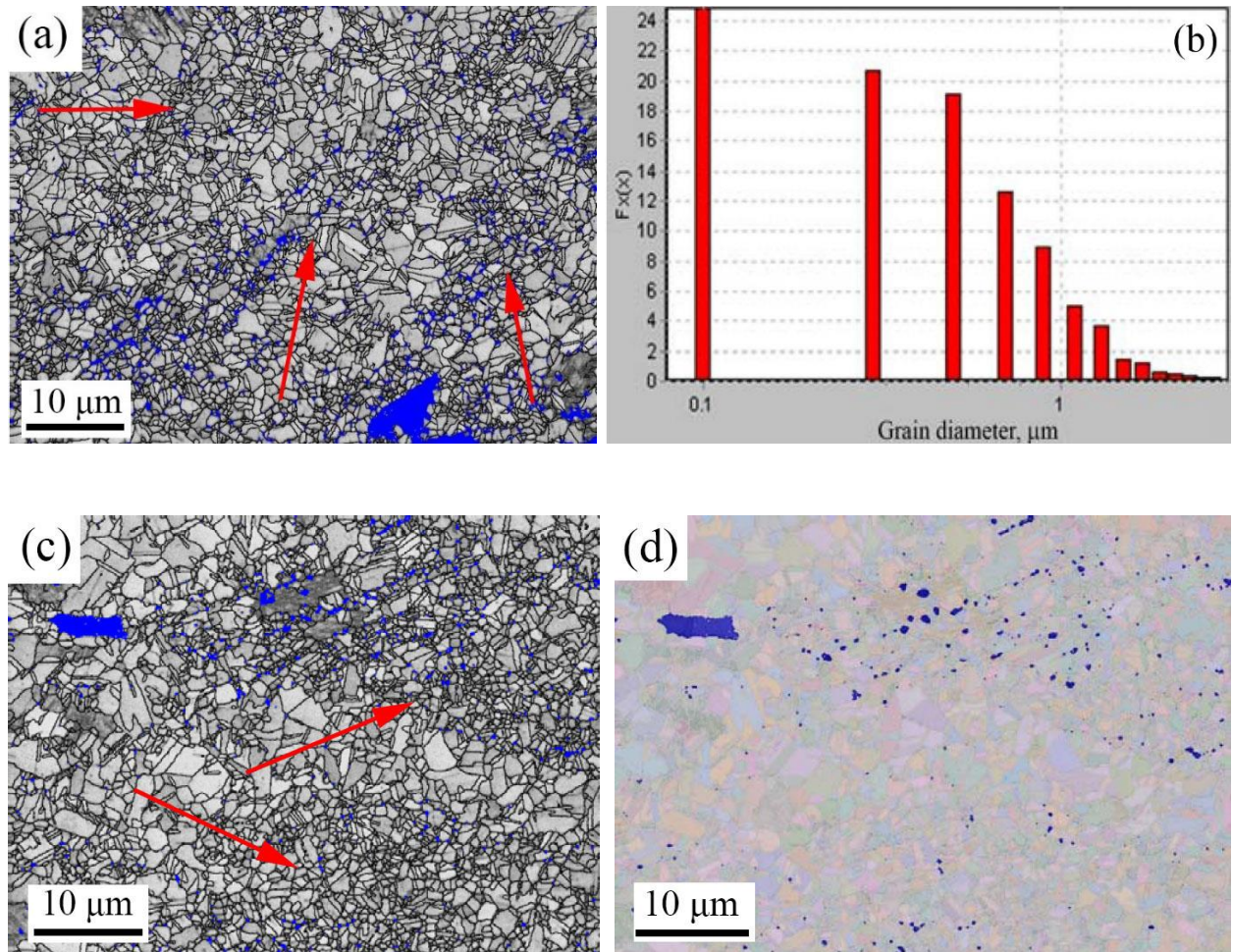

Fig. 4. Fast-heating annealing microstructures, (a) Image-quality contrast map overlapped with phase map of the microstructure achieved at 650°C/180 s, (b) Grain size distribution of the corresponding structure in (a), (c) IQ-contrast map and phase map of the microstructure achieved at 700°C/180 s, (d) Phase map revealing the ferrite phase distribution of the structure in (c). (Austenite γ–fcc in grey, ferrite α-bcc in blue).

The microstructures obtained in FH annealing at higher temperatures of 1000 and 1100 °C with a short duration of 2 s are presented in Fig. 5. Qualitatively, the structures obtained are similar as formed at the lower temperatures, consisting austenite as a major phase with some globular ferrite grains, but the grain size is distinctly coarser for the both phases (Table 1).
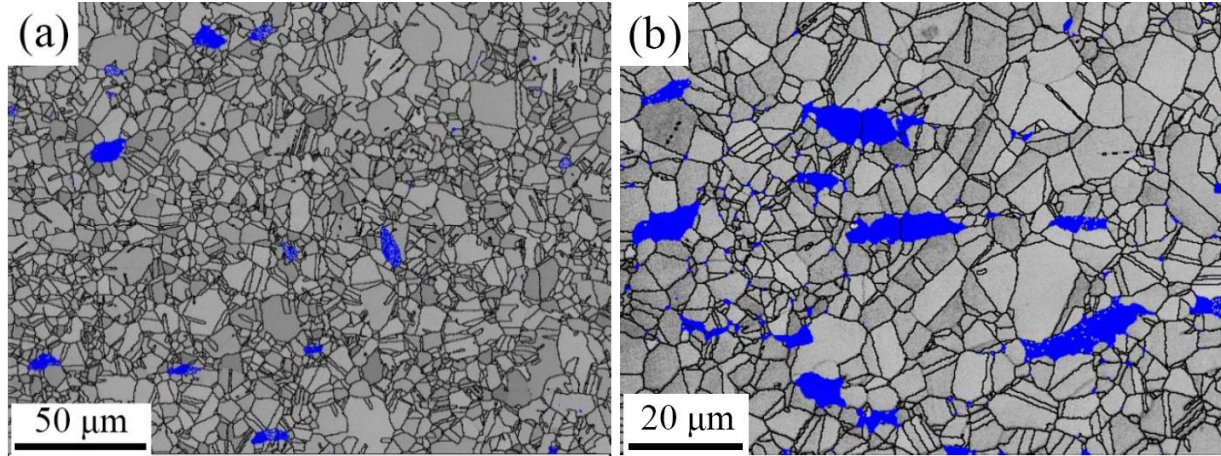

Fig. 5. Overlapped EBSD-IQ and phase maps of the microstructures achieved by fast-heating annealing for 2 s at: (a) 1000 °C, and (b) 1100 °C. (austenite γ–fcc in grey, ferrite α-bcc in blue).

Table 1. Microstructural characteristics of the Fe-21Mn-3-Al-3Si steel annealed at different temperatures and times

Temp., °C/ t, s	Ferrite Fraction	Grain Size, μm	
		Ferrite	Austenite
650/180	0.07	0.2	0.8
700/180	0.06	0.23	1
1000 /2	0.035	3.5	4
1100 /2	0.07	6	9
1200 /2	0.67	85	30

However, the structure formed at 1200 °C is different consisting much higher amount of ferrite (about 67%), as shown in Fig. 6. Also, it is worth noting that the shape of ferrite grains after

annealing at this temperature is not globular but equiaxed. Higher-magnification EBSD map, Fig. 6(b), shows that some of ferrite grain boundaries are decorated by austenite particles. Those particles are nucleated and formed on the ferrite grain boundaries by the massive transformation, since grain boundaries are favourable nucleation sites for austenite transformation during the fast cooling to room temperature.
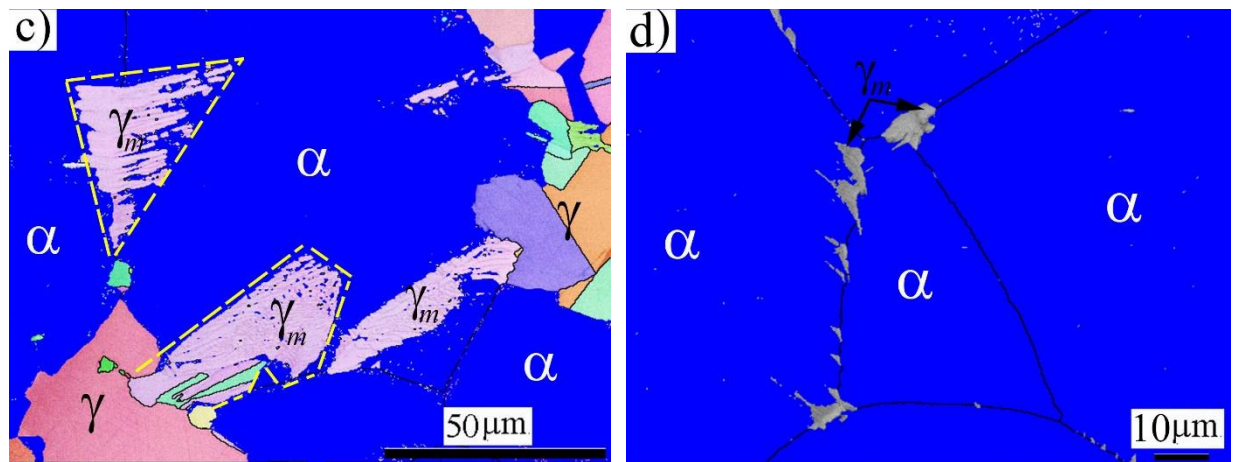

Fig. 6. Microstructures obtained by fast-heating annealing at 1200 °C for 2 s showing: (a) duplex ferrite and austenite (Orientation imaging microscopy map for austenite overlapped with phase map) and (b) high magnification of austenite nucleation and growth on ferrite grain boundaries (ferrite α-bcc in blue, austenite γ-fcc in grey).

3.3. Tensile Tests

The tensile true stress-strain curves for different structures of the investigated steel are shown in Fig. 7. As the annealing temperature increased from 650 and 700 °C to 1000 and 1100 °C, the steel showed obviously lower yield and ultimate strengths with higher elongations. However, the specimen annealed at the highest temperature of 1200 °C revealed definitely higher flow stress than those annealed at 1000 and 1100 °C. Furthermore, it is evident from the flow curves that this sample has also a superior strain hardening rate compared to its counterparts annealed at 1000 and 1100 °C.
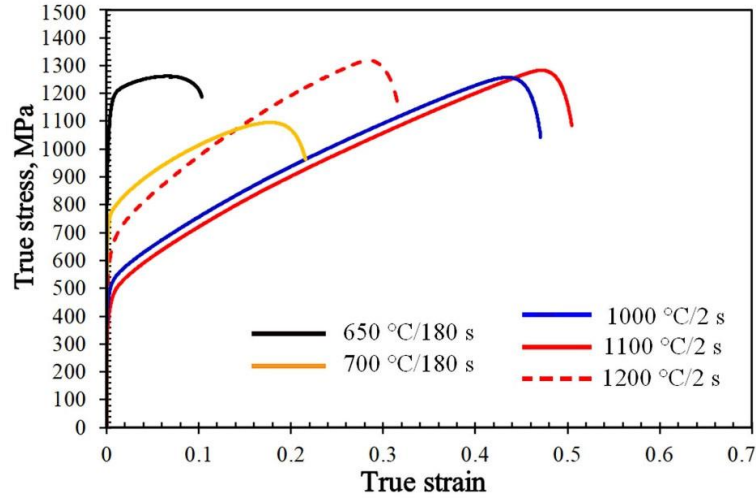
Fig. 7. Room temperature true stress-strain curves of the steel with different grain structures obtained at different fast-heating annealing conditions.

3.4. Modeled flow stress curves

The phenomenological model, presented in Section 2.5, was used to further analyze the mechanical behavior of the present TWIP steel. In this regard, two annealing conditions, i.e. 1200 °C/2 s and 1000 °C/2 s, which correspond to the maximum and minimum fractions of ferrite, respectively (Table 1) were selected for modeling. The model parameters were either determined based on the experimental data in the present work or extracted from the literature (Table 2). As demonstrated in Fig. 8, the predicted stress-strain data showed good agreement with the experimental flow curves.

Table 2. Model parameters for the flow behavior of the steel after two recrystallization conditions.

Parameter	Recrystallization condition		Determination
	1200 °C/2 s	1000 °C/2 s	
F_0	0.25	0.22	[40]
M	3.06	3.06	[29]
Ω	7.786	18.982	Fitting
U (/m^2)	1.2×10^{15}	1.35×10^{15}	Fitting
R	1.3	0.5	Fitting

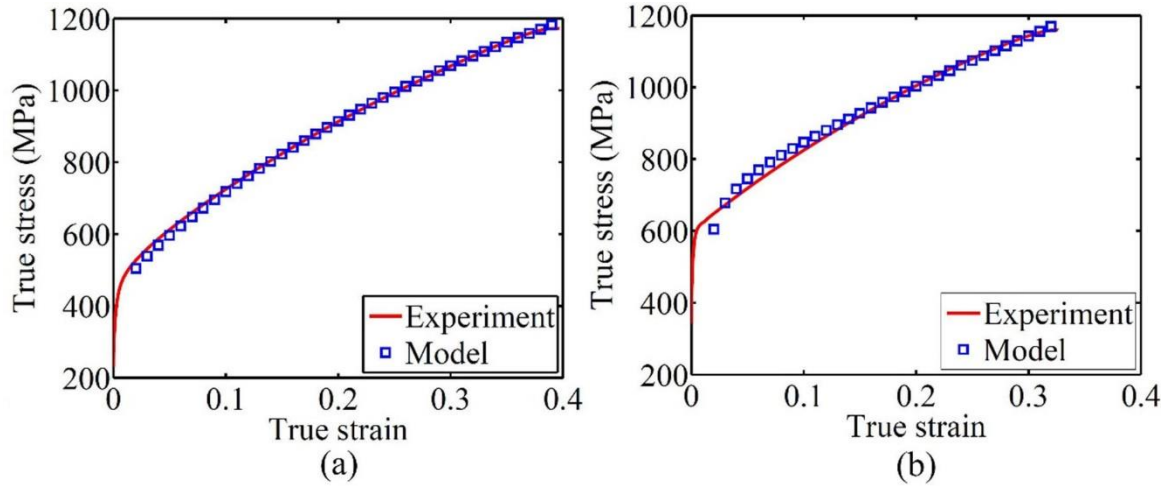| σ_0 (MPa)	450	560	Experimental
α	0.4	0.4	[29]
α'	0.9	0.9	[41]
b (m)	2.5×10^{-10}	2.5×10^{-10}	[32, 29]
β	4.84	5.93	Fitting
t (nm)	260	260	[40]
d_{aus} (μm)	30	4	Experimental
d_{fer} (μm)	85	4	Experimental
f_{aus}	0.33	0.965	Experimental
f_{fer}	0.67	0.035	Experimental
G (GPa)	65	65	[29]
H (/m)	2.2×10^8	5×10^7	Fitting
m	2.2510	2.2500	Fitting
W	126 b	126 b	[29]
n_0	4	4	[29]

Fig. 8. Comparison between model and the experimental flow curves for specimens fast-heating annealed at a) 1000 °C/2 s, b) 1200 °C/2 s.

4. Discussion

4.1. Cast material

The equilibrium phase(s) which appear after solidification of the steel can be concluded from an isothermal section of the Fe-Mn-Al phase diagram at 1000 °C shown in Fig. 9a, taken from Ref. [33], as well as from Thermo-Calc analysis. The location of the Fe-21Mn-3Al steel is highlighted by a red circle in the isothermal section and it indicates that the steel of the present composition (without Si) should be fully austenitic. The equilibrium phase diagram for the chemical composition of the studied Fe-21.3Mn-0.01C-3Al-3Si steel, constructed by Thermo-Calc analysis (TCFE 9 database) is plotted in Fig. 9b. From this, it is apparent that the α-bcc ferrite phase is predicted to be thermodynamically stable at temperatures higher than 1120 °C and its fraction increases gradually to 0.5 at 1200 °C and 1.0 (fully ferritic) at 1260 °C.

According to Fig. 9b, the only equilibrium phase at room temperature is then predicted to be γ-*fcc* (austenite). However, the cast structure, Fig. 2, exhibits austenitic matrix containing a small volume fraction of ferrite (α-*bcc*). It is well known that addition of Si to the Fe-Mn-Al system can affect the formation of ferrite phase [34]. In case of high Al content, adding Si would promote ferrite.
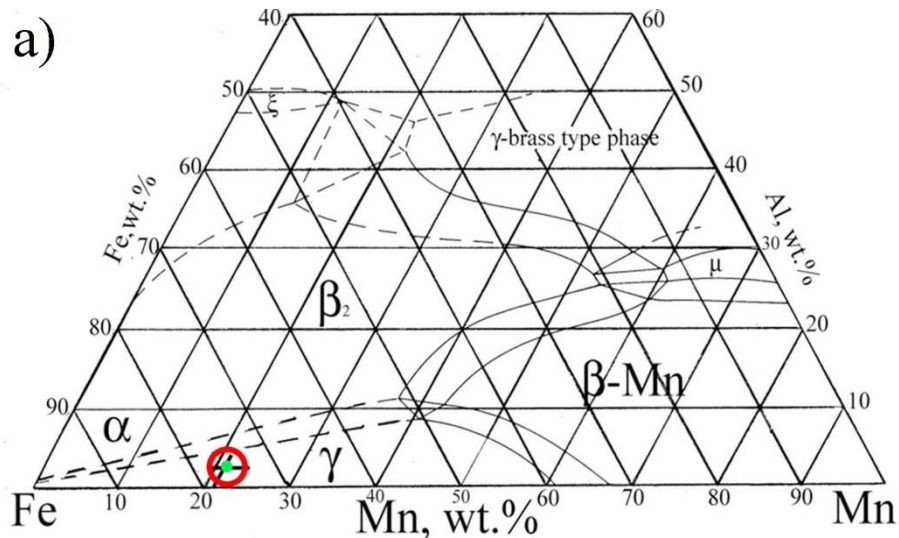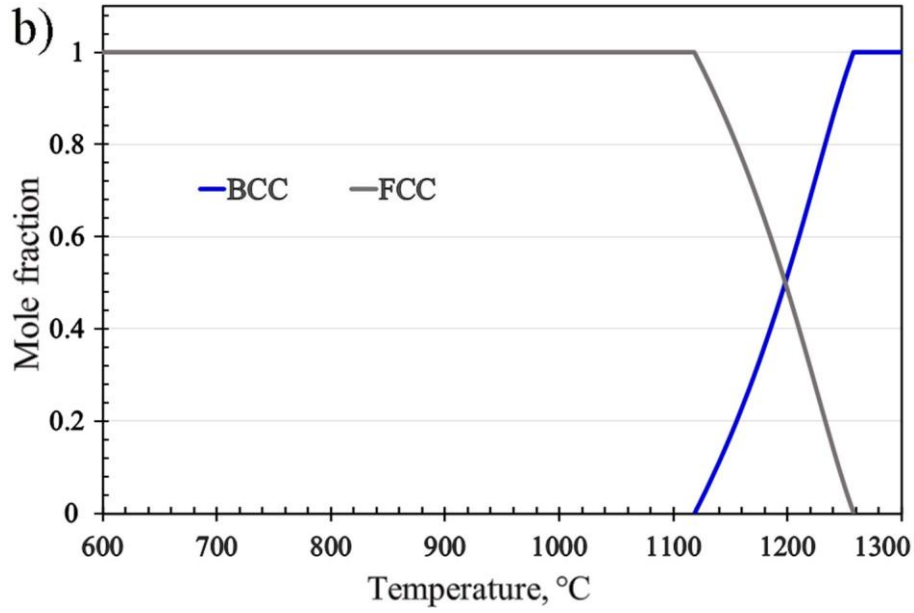
Fig. 9. (a) Isothermal cross-sections of Fe-Mn-Al system at 1000°C [33], (b) Isopleth equilibrium phase diagram for the Fe-21.3Mn-0.01C-3Al-3Si steel, predicted by Thermo-Calc analysis (using TCFE 9 database).

In order to further investigate the presence of ferrite in the cast steel, possible partitioning of the alloying elements was also examined. The partition ratio, P_D, *i.e.*, the ratio of the concentration of an element in ferrite to that in the adjacent austenite, was calculated based on EDS analysis of the both phases. While partition ratios of Al and Si were ~1.62 and 1.18, respectively, a less than unity value (~ 0.7) was measured for P_D of Mn. Thus, it is evident that Al and Si are preferentially partitioned into ferrite, but austenite is enriched in Mn.

In a previous work [35], it was shown that an Fe-0.22C-24Mn-6Al-0.48Si steel has fully austenitic structure at room temperature, even though that steel contained a higher Al content but also higher C and Mn than the present alloy had. On the other hand, in another study by Frommeyer et al. [36], a steel with the composition Fe-0.04C-20Mn-3Al-3Si (wt. %) displayed a duplex microstructure of γ-*fcc* + ε-martensite without ferrite. Also, in a recent work, Hamada et al. [37] reported that a high Si content of 2.4 wt.% promoted ferrite formation in micro-alloyed TWIP-type stainless steel. Therefore, we can conclude that the presence of ferrite in the present cast TWIP steel can be attributed to the relatively high Si and Al contents together with the low C content.

4.2. Microstructural evolution during annealing

As depicted in the Fig. 4, the specimens which were annealed at the lower temperatures (650 and 700 °C) consisted of fine austenitic structure with small fractions of ferrite. In both specimens there existed bands/regions along which definitely finer grains are observed (shown by arrows in Figs. 4(a) and (c)). This indicates that at these low temperatures, the annealed specimens are accompanied by some inhomogeneity in the grain structure. The inhomogeneity can also be related to the fact that the annealed microstructure is inherited from different prior ferrite and austenite grains (the initial duplex structure). Similar structures consisting of ultrafine-grained island with coarser grains have been reported after the reversion annealing of Fe-18Cr-7Ni austenitic stainless steel, resulting from inhomogeneous distribution (banding) of Mn [38]. Thus, Mn segregation can be another origin for the different grain sizes observed in the present investigated steel.

Similar phase structure (mainly austenitic with some globules of ferrite) but with definitely coarser grains was achieved after FH annealing at the higher temperatures of 1000 and 1100 °C (Fig. 5). However, as the annealing temperature was increased to 1200 °C, a high fraction of ferrite appeared in the microstructure (Fig. 6). It is clear from this microstructure that the sample was heated into the duplex phase region where the austenite which existed at temperatures below 1120 °C has partly transformed to ferrite during heating and soaking (see Fig. 9b). In the FH annealing cycle, we employed a fast cooling rate ~ 200 °C/s to ensure minimal transformation during the cooling step after isothermal holding. However, two different morphologies of the austenite phase can be observed in the microstructure formed at 1200 °C (Fig. 6(a)). While large polygonal austenitic grains with different orientations (different colors) are evident, there are also irregular massive austenite grains (γ_m) with planar and curved boundaries, highlighted by yellow dashed borders. These were located on the ferrite grain boundaries and grew into the ferrite grains (Fig. 6(b)). These irregular austenite grains γ_m are produced by rapid conversion of ferrite to austenite by the massive transformation during quenching or fast cooling, as reported by Cheng and Lai [39].

It can be observed that regularly shaped prior austenite grains bearing annealing twins are also present in the FH annealed microstructure.

4.3. Mechanical properties

True stress-strain diagrams of the experimental material after FH annealing at various conditions were presented in Fig. 7. The mechanical properties extracted from these diagrams are given in Fig. 10. The typical ultimate tensile strength (UTS) values of 25Mn3Al and 25Mn3Al3Si TWIP steels taken from Ref. [40] are also presented for comparison. The microstructures of both steels taken from [40] were fully austenitic γ-fcc structure with equiaxed grains and an average grain size of 150 μm.
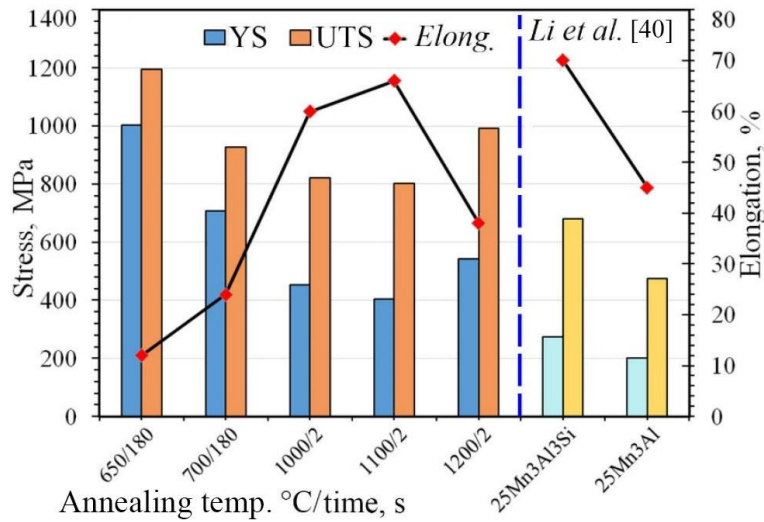

Fig. 10. Mechanical properties extracted from the stress-strain curves: yield strength (*YS*), ultimate tensile strength (*UTS*), and elongation. Data of 25Mn3Al and 25Mn3Al3Si are taken from Ref. [40].

It can be observed that the overall performance of the steel processed by FH annealing in the present work at 1000–1200 °C is superior compared to the 25Mn3Al and 25Mn3Al3Si steels in the referred work. Whereas the yield strength (*YS*) values are 200 MPa and 275 MPa for the 25Mn3Al and 25Mn3Si3Al steels [40], the FH structures achieved at 1000, 1100 and 1200 °C here exhibit significantly higher YS values, i.e. 450, 400 and 540 MPa, respectively. Similarly, the specimens FH annealed at the high temperatures 1000, 1100, and 1200 °C, exhibited higher UTS values, 820, 800 and 1000 MPa, respectively, while the UTS values of 25Mn3Al and 25MN3Al3Si steels were reported to be 475 and 680 MPa, respectively [40]. This is attributed to the striking grain refinement enhanced by FH annealing. Similar results are recently observed by Cerda et al. [41] who applied

ultra-fast heating rates up to 1500 °C/s on cold-rolled carbon steels. They reported a significant grain refining caused by the FH annealing in these steels as well. Furthermore, they found that the improvement in the mechanical properties was also linked to the obtained phase constituents, i.e. increasing contents of ferrite and bainite due to the rapid heating.

It should be noted that the YS values of the structure processed by FH annealing at 1200 °C is higher than those structures processes at 1000 and 1100 °C. It is well known that the YS of an annealed steel is directly related to the alloying concentrations, grain size and the phase constituents. All the structures processed by FH have the same alloying concentrations but different grain sizes. Usually, larger grain sizes are expected at higher annealing temperatures. Although the structure processed at 1200 °C exhibited a coarser grain structure (see Table 1, Figs. 5 and 6), it showed higher YS and UTS values. This is attributed to the high content of the harder phase (α-bcc) in the structure. This was further confirmed by microhardness measurements of the austenite and ferrite phases using a Vickers hardness tester. The ferrite phase was found to exhibit significantly higher hardness with the average of 292 ± 12 HV than the austenite phase, 186 ± 14 HV. This is mainly attributed to the hardening effects due to the high Al and Si contents in the ferrite phase (*see* the partition ratios of Al and Si in Section 4.1). Similar behaviour was found in one of our previous work where the ferrite phase in high-Mn TWIP steel bearing high-Al content was much harder than the austenite phase due to the solid solution strengthening effects of Al and Si [35].

The elongation values of the structures processed at 1000 and 1100 °C are comparable with those of 25Mn3Al3Si, i.e. high values of over 60%, see Fig. 10. This property can be simply attributed to the larger austenitic grain sizes connected with lower twinning stresses [11, 42], so that the TWIP mechanism can act as a barrier against the growth of possible micro-necking and hence leads to increased ductility.

From these properties, it can be concluded that the FH-annealing is a potential process to control the grain structure and the phase constituents, and consequently to improve the mechanical properties. Furthermore, it reduces energy consumption in steel manufacturing, compared to the conventional long annealing treatment processes.

4.4. Physically based model

In order to survey the influence of mechanical twinning on the flow stress of the studied steel, the length scale parameter for austenitic regions, i.e. L in Eq. (3), is plotted in Fig. 11(a) versus the applied true strain. This parameter shows the mean free path for the movement of dislocations. Expectedly, the parameter L is initially much smaller in the specimen with a finer grain size, i.e. the one recrystallized at 1000 °C. However, with the progress of deformation, mechanical twins form and consequently the parameter L rapidly decreases in the coarse-grained specimen recrystallized at 1200 °C. In other words, the influence of twinning on the reduction of the mean free path is more pronounced in the coarser grain structure. Furthermore, mechanical twinning is much more intense in the specimens with coarser grains, which has been ascribed to the influence of grain boundaries on increasing the nucleation stress for twinning [11, 10]. Consistently, as the present model shows, the slope of L versus true strain is much higher for the coarser grained specimen (1200 °C). As a consequence, slightly different trends are seen for the kinematic hardening of the two specimens (Fig. 11b). Up to the true strain of ~ 0.15, the slope of σ_2 vs. ε shows an increasing trend for the coarse-grained specimen, while a decreasing slope is seen for the fine-grained specimen. However, in the whole range of the applied strain, the influence of kinematic hardening is higher for the fine-grained specimen, recrystallized at 1000 °C.
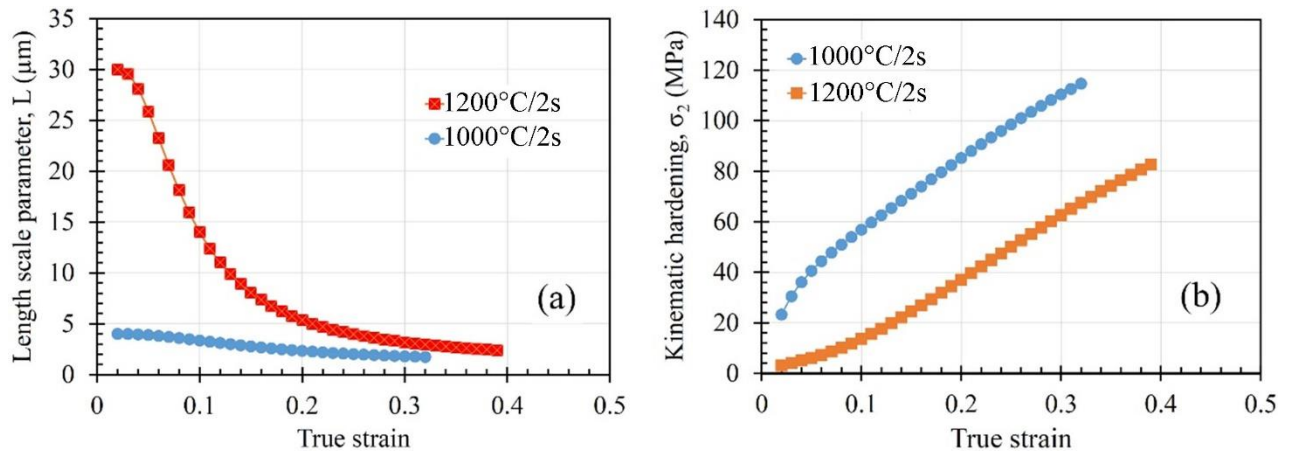

Fig. 11. The variation of (a) length scale parameter and (b) the kinematic hardening with the applied strain.

By solving the differential Eqs. (2) and (8), the evolution of dislocation density in the austenite and ferrite phases is plotted as a function of true strain for both the modeled specimens (Fig. 12). The rates of increase of dislocation density in the austenite regions are clearly higher than in those of ferrite. This can be related to the influence of length scale parameter (L) in the corresponding equation of austenite (Eq. (2)), while it is not included in the equation used for ferrite (Eq. (8)). Furthermore, the dislocation density of austenite in the specimen which was recrystallized at 1200 °C increases more rapidly than that in the specimen recrystallized at 1000 °C, due to the higher rate of reduction of L in the former specimen (see Fig. 11(a)).
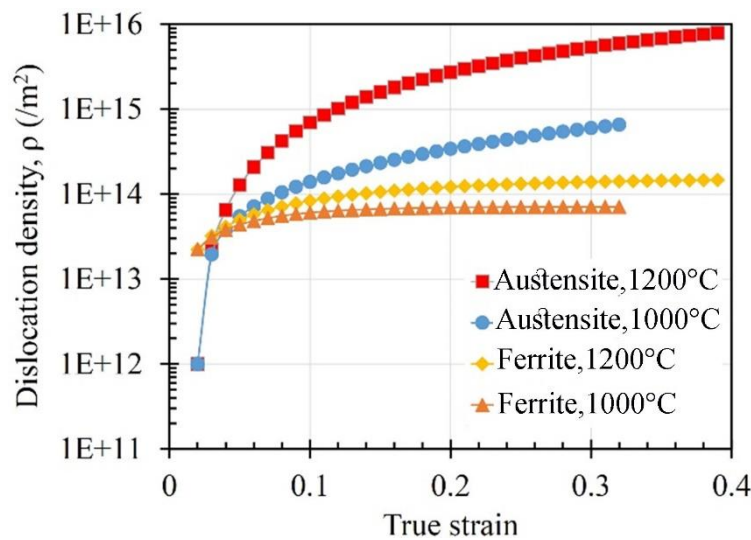

Fig. 12. Evolution of dislocation density in ferrite and austenite phases of the specimens fast-heating annealed at 1000 and 1200 °C for 2 s.

Finally, considering the phase fractions of each specimen, the contributions of isotropic and kinematic hardening in the total flow stress is calculated based on the physically based model (Fig. 13). While the contribution of kinematic hardening in the specimen, which was recrystallized at 1000 °C, reaches ~10% of the total stress, the kinematic contribution for the coarse-grained specimen recrystallized at 1200 °C is minor. According to Fig. 11a, in the whole range of the applied strain, the length scale parameter is smaller in the fine-grained specimen. On the other hand, mechanical twinning leads to a very rapid decrease of mean free path in the austenitic regions of

coarse-grained specimen. However, the fraction of austenite in the latter specimen is much lower than the former which lowers the contribution of twinning in the coarse-grained specimen.
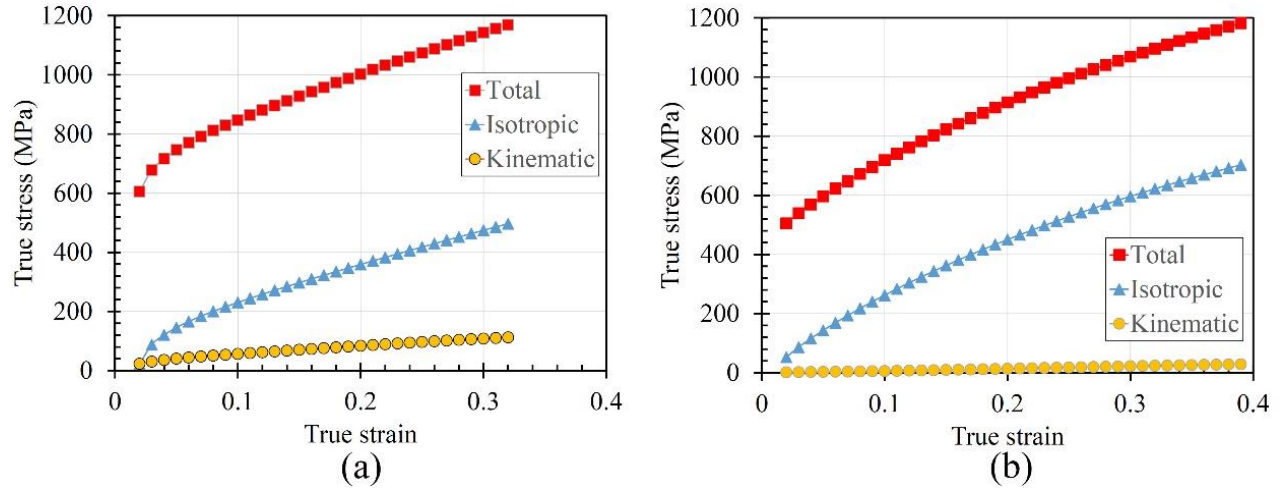

Fig. 13. The contributions of isotropic and kinematic hardening (σ_1, σ_2) in the total flow stress of the specimen fast-heating annealed at (a) 1200 °C and (b) 1000 °C, based on the model.

5. Conclusions

In the present work, a cold-rolled high-Mn TWIP-type steel, Fe-0.01C-21Mn-3Al-3Si, was undergone short fast-heating annealing with a heating rate of 200 °C/s to promote grain refinement and control the phase constituents in the achieved microstructures. Consequently, the correlated mechanical properties could be improved. Furthermore, a phenomenological model was used to predict the flow stress behavior of the FH annealed structures based on the microstructural evolution at different annealing temperatures. The following main conclusions can be drawn:

1. The fast-heating annealing at the temperatures 1000 and 1100 °C for 2 s resulted in fine grain structures with equiaxed austenite grains and minimal fraction of ferrite. However, the FH annealing at 1200 °C changed significantly the phase constituents due to the austenite to ferrite transformation during holding at 1200 °C and massive transformation from ferrite to austenite during fast cooling.

2. Higher tensile strengths (up to 1200 MPa) were reached in specimens recrystallized at the lower temperature of 700 °C, but the ductility remained much lower in these structures. This could be ascribed to inhomogeneity of the microstructure formed at lower temperatures.

3. From the processed microstructure by FH annealing at 1200 °C, it can be concluded that holding temperature and time as well as the cooling rate were feasible to obtain a duplex microstructure consisting of hard ferrite and softer austenite and thereby to achieve a good combination of strength and ductility (yield and tensile strengths 540 and 1000 MPa, respectively and the elongation as high as 35%).

4. The phenomenological model based on Bergstrom's equations, can correctly predict the flow behavior of the structures processed by the FH annealing. With the progress of deformation in the grain structure achieved at 1200 °C, the mean free path of dislocations decreased more rapidly. As the result, an increasing trend was seen for the directional (kinematic) hardening especially at small strains (up to 0.15). On the other hand, in case of the specimen annealed at 1000 °C, with a finer grain structure (4 μm) and higher austenite content of 97%, the influence of mechanical twins on reduction of the mean free path of dislocations was much higher suggesting a higher contribution of kinematic hardening.

References

[1] J. Dai, Q. Meng and H. Zheng, "High-strength dual-phase steel produced through fast-heating annealing method," *Results in Materials,* vol. 5, p. 100069, 2020.

[2] Y. G. Deng, Y. Li, H. Di and R. D. K. Misra, "Effect of heating rate during continuous annealing on microstructure and mechanical properties of high-strength dual-phase steel," *Journal of Materials Engineering and Performance,* vol. 28, pp. 4556-4564, 2019.

[3] L. S. Thomas and D. K. Matlock, "Formation of banded microstructures with rapid intercritical annealing of cold-rolled sheet steel," *Metallurgical and Materials Transactions A,* vol. 49, pp. 4456-4473, 2018.

[4] Q. Meng, J. Li and H. Zheng, "High-efficiency fast-heating annealing of a cold-rolled dual-phase steel," *Materials & Design,* vol. 58, pp. 194-197, 2014.

[5] F. Vercruysse, F. M. Castro Cerda, P. Verleysen and R. H. Petrov, "Behavior of ultrafast annealed advanced high strength steels under static and dynamic conditions," *Materials Science & Engineering A,* vol. 780, p. 139168, 2020.

[6] D. C. Xu, J. Li, Q. G. Meng, Y. D. Liu and P. Li, "Effect of heating rate on microstructure and mechanical properties of TRIP-aided multiphase steel," *Journal of Alloys and Compounds,* vol. 614, pp. 94-101, 2014.

[7] G. Liu, S. Zhang, J. Li, J. Wang and Q. Meng, "Fast-heating for intercritical annealing of cold-rolled quenching and partitioning steel," *Materials Science and Engineering A,* vol. 669, pp. 387-395, 2016.

[8] D. De Knijf, A. Puype, C. Föjer and R. Petrov, "The influence of ultra-fast annealing prior to quenching and partitioning on the microstructure and mechanical properties," *Materials Science and Engineering A,* vol. 627, pp. 182-190, 2015.

[9] M. A. Valdes-Tabernero, A. Kumar, R. H. Petrov, M. A. Monclus, J. M. Molina-Aldareguia and I. Sabirov, "The sensitivity of the microstructure and properties to the peak temperature in an ultrafast heat treated low carbon-steel," *Materials Science & Engineering A,* vol. 776, p. 138999, 2020.

[10] R. Ueji, N. Tsuchida, D. Terada, N. Tsuji, Y. Tanaka, A. Takemura and K. Kunishige, "Tensile properties and twinning behavior of high manganese austenitic steel with fine-grained structure," *Scripta Materialia,* vol. 59, pp. 963-966, 2008.

[11] K. M. Rahman, V. A. Vorontsov and D. Dye, "The effect of grain size on the twin initiation stress in a TWIP steel," *Acta Materialia,* vol. 89, pp. 247-257, 2015.

[12] Y. Z. Tian, Y. Bai, L. J. Zhao, S. Gao, H. K. Yang, A. Shibata, Z. F. Zhang and N. Tsuji, "A novel ultrafine-grained Fe22Mn0.6C TWIP steel with superior strength and ductility," *Materials Characterization,* vol. 126, pp. 74-80, 2017.

[13] X. Yuan, L. Chen, Y. Zhao, H. Di and F. Zhu, "Influence of annealing temperature on mechanical properties and microstructures of a high manganese austenitic steel," *Journal of Materials Processing Technology,* vol. 217, pp. 278-285, 2015.

[14] P. Lan and J. Zhang, "Tensile property and microstructure of Fe-22Mn-0.5C TWIP steel," *Materials Science and Engineering: A,* vol. 707, pp. 373-382, 2017.

[15] D. Fabregue, O. Bouaziz and D. Barbier, "Nano-twinned steel exhibits high mechanical properties obtained through ultra-rapid heat treatment," *Materials Science and Engineering: A,* vol. 712, pp. 765-771, 2018.

[16] K. Wang, A. Wei, Z. Shi, X. Chen, J. Lin, X. Tong, Z. Tao and X. Chen, "The preparation and performance of grain size gradient TWIP steel fabricated by laser heat treatment," *Materials Science and Engineering A,* vol. 743, pp. 294-300, 2019.

[17] P. Dastur, A. Zarei-Hanzaki, M. H. Pishbin, M. Moallemi and H. R. Abedi, "Transformation and twinning induced plasticity in an advanced high Mn austenitic steel processed by martensite reversion treatment," *Materials Science and Engineering: A,* vol. 696, pp. 511-519, 2017.

[18] S. -M. Lee, S. -J. Lee, S. Lee, J. -H. Nam and Y. -K. Lee, "Tensile properties and deformation mode of Si-added Fe-18Mn-0.6C steels," *Acta Materialia,* vol. 144, pp. 738-747, 2018.

[19] M. Bambach, S. Heppner, D. Steinmetz and F. Roters, "Assessing and ensuring parameter identifiability for a physically-based strain hardening model for twinning-induced plasticity," *Mechanics of Materials,* vol. 84, pp. 127-139, 2015.

[20] B. C. De Cooman, Y. Estrin and S. K. Kim, "Twinning-induced plasticity (TWIP) steels," *Acta Materialia,* vol. 142, pp. 283-362, 2018.

[21] J. H. Kang, T. Ingendahl and W. Bleck, "A constitutive model for the tensile behaviour of TWIP steels: Composition and temperature dependencies," *Materials & Design,* vol. 90, pp. 340-349, 2016.

[22] F. Liu, W. J. Dan and W. G. Zhang, "Strain hardening model of twinning induced plasticity steel at different temperatures," *Materials & Design,* vol. 65, pp. 737-742, 2015.

[23] G. Joo and H. Huh, "Rate-dependent isotropic–kinematic hardening model in tension–compression of TRIP and TWIP steel sheets," *International Journal of Mechanical Sciences,* Vols. 146-147, pp. 432-444, 2018.

[24] G. B. Olson and M. Cohen, "A general mechanism of martensitic nucleation: part I. General concepts and the FCC-HCP transformation," *Metallurgical Transactions A,* vol. 7, pp. 1897-1904, 1976.

[25] A. Khosravifard, M. M. Moshksar and R. Ebrahimi, "High strain rate torsional testing of a high manganese steel: Design and simulation," *Materials and Design,* vol. 52, pp. 495-503, 2013.

[26] G. Joo, H. Huh and J. Kwon, "Evaluation of rate-dependent hardening behaviors of AHSS sheets with novel tension and compression test devices," *Journal of Materials Processing Technology,* vol. 270, pp. 365-379, 2019.

[27] U. F. Kocks and H. Mecking, "Physics and phenomenology of strain hardening: the FCC case," *Progress in Materials Science,* vol. 48, pp. 171-273, 2003.

[28] Y. Estrin and H. Mecking, "A unified phenomenological description of work hardening and creep based on one-parameter models," *Acta Metallurgica,* vol. 32, pp. 57-70, 1984.

[29] O. Bouaziz, S. Allain and C. Scott, "Effect of grain and twin boundaries on the hardening mechanisms of twinning-induced plasticity steels," *Scripta Materialia,* vol. 58, pp. 484-487, 2008.

[30] A. Mejía, F. Reyes-Calderón and J. M. Cabrera, "Modeling the hot flow behavior of a Fe–22Mn–0.41C–1.6Al–1.4Si TWIP steel microalloyed with Ti, V and Nb," *Materials Science and Engineering: A,* vol. 644, pp. 374-385, 2015.

[31] A. S. Hamada, A. Khosravifard, A. P. Kisko, E. Ahmed and D. A. Porter, "High temperature deformation behavior of a stainless steel fiber-reinforced copper matrix composite," *Materials Science and Engineering: A,* vol. 669, pp. 469-479, 2016.

[32] S. V. Mehtonen, L. P. Karjalainen and D. A. Porter, "Modeling of the high temperature flow behavior of stabilized 12–27 wt% Cr ferritic stainless steels," *Materials Science and Engineering: A,* vol. 607, pp. 44-52, 2014.

[33] X. J. Liu, S. M. Hao, L. Y. Xu, Y. F. Guo and H. Chen, "Experimental study of the phase equilibria in the Fe-Mn-Al system," *Metallurgical and Materials Transactions A,* vol. 27, p. 2429–2435, 1996.

[34] T. F. Liu, J. S. Chou and C. C. Wu, "Effect of Si addition on the microstructure of an Fe-8.0Al-29.0Mn-0.90C alloy," *Metallurgical Transactions A,* vol. 21, pp. 1891-1899, 1990.

[35] A. S. Hamada, L. P. Karjalainen and M. C. Somani, "Constitutive behaviour of two high Mn-Al TWIP steels at hot rolling temperatures," *Canadian Metallurgical Quarterly,* vol. 46, pp. 47-56, 2007.

[36] G. Frommeyer, U. Brux and P. Neumann, "Super-ductile high-strength manganese TRIP/TWIP steels for high energy absorption purposes," *ISIJ International,* vol. 43, p. 438, 2003.

[37] A. Hamada, T. Juuti, A. Khosravifard, A. Kisko, P. Karjalainen, D. Porter and J. Komi, "Effect of silicon on the hot deformation behavior of microalloyed TWIP-type stainless steels," *Materials & Design,* vol. 154, pp. 117-129, 2018.

[38] A. Järvenpää, M. Jaskari, J. Man and L. P. Karjalainen, "Austenite stability in reversion-treated structures of a 301LN steel under tensile loading," *Materials Characterization,* vol. 127, pp. 12-26, 2017.

[39] W. C. Cheng and C. K. Lai, "Observing massive phase transformation in a Fe–Mn–Al alloy," *Scripta Materialia,* vol. 55, pp. 783-786, 2006.

[40] D. Li, Y. Feng, S. Song, Q. Liu, Q. Bai, F. Ren and F. Shangguan, "Influences of silicon on the work hardening behavior and hot deformation behavior of Fe–25 wt%Mn–(Si, Al) TWIP steel," *Journal of Alloys and Compounds,* vol. 618, pp. 768-775, 2015.

[41] F. M. C. Cerda, B. Schulz, D. Celentano, A. Monsalve, I. Sabirov and R. H. Petrov, "Exploring the microstructure and tensile properties of cold-rolled low and medium carbon steels after ultrafast heating and quenching," *Materials Science and Engineering A,* vol. 745, pp. 509-516, 2019.

[42] J. Chen, F. T. Dong, H. I. Jiang, Z. Y. Liu and G. D. Wang, "Influence of final rolling temperature on microstructure and mechanical properties in a hot-rolled TWIP steel for cryogenic application," *Materials Science and Engineering: A,* vol. 724, pp. 330-334, 2018.